

Highly ordered arrangement of single neurons in orientation pinwheels

Kenichi Ohki¹, Sooyoung Chung^{1†}, Prakash Kara^{1†}, Mark Hübener², Tobias Bonhoeffer² & R. Clay Reid¹

In the visual cortex of higher mammals, neurons are arranged across the cortical surface in an orderly map of preferred stimulus orientations^{1,2}. This map contains ‘orientation pinwheels’, structures that are arranged like the spokes of a wheel such that orientation changes continuously around a centre. Conventional optical imaging^{3,4} first demonstrated these pinwheels^{3,5}, but the technique lacked the spatial resolution to determine the response properties and arrangement of cells near pinwheel centres. Electrophysiological recordings later demonstrated sharply selective neurons near pinwheel centres^{6,7}, but it remained unclear whether they were arranged randomly or in an orderly fashion. Here we use two-photon calcium imaging *in vivo*^{8–12} to determine the microstructure of pinwheel centres in cat visual cortex with single-cell resolution. We find that pinwheel centres are highly ordered: neurons selective to different orientations are clearly segregated even in the very centre. Thus, pinwheel centres truly represent singularities in the cortical map. This highly ordered arrangement at the level of single cells suggests great precision in the development of cortical circuits underlying orientation selectivity.

A smooth map for orientation preference in the mammalian visual cortex was first demonstrated by Hubel and Wiesel^{1,2}, who recorded from neurons along electrode penetrations parallel to the cortical surface. They found occasional abrupt discontinuities in the sequence of preferred orientations, but point-by-point sampling with microelectrodes did not permit an overall characterization of the orientation map. Only several decades later did optical imaging of intrinsic signals reveal that the orientation preference map is composed of pinwheel-like structures^{3,5}. Primarily as a result of light scatter in cortical tissues, conventional optical imaging^{3,4} has a lateral spatial resolution of 50 μm at best¹³, and very limited depth resolution, so it is not capable of resolving the fine-scale structure of the pinwheel centres. Similarly, previous electrophysiological studies of pinwheel centres⁶ could not localize neurons precisely (for instance, tetrodes record in a region with a radius of about 65 μm (ref. 14)). Thus, below this spatial scale, they could not resolve whether neurons selective for different orientations were arranged randomly near the pinwheel centre or might be perfectly segregated (see Supplementary Fig. S1). Two-photon calcium imaging^{8–12} permits functional mapping at single-cell resolution¹⁰ in three dimensions, so it is ideally suited to resolve this question.

To target the injection of the calcium indicator dye to a pinwheel centre, we first recorded maps of preferred orientation in area 18 of cat visual cortex (postnatal days 28–35) with intrinsic-signal optical imaging (Fig. 1a). An injection of Oregon Green BAPTA-1 acetoxymethyl ester (AM) at a pinwheel site typically labelled thousands of neurons in a region with a diameter of 300–600 μm . Two-photon calcium imaging permitted the simultaneous measurement of the

visual responses of tens to hundreds of labelled neurons within a given optical cross-section parallel to the cortical surface.

When we measured calcium signals evoked by visual stimuli (gratings at four different orientations, each drifting in two opposite directions), we found that neurons responsive to each orientation and direction were tightly clustered around a pinwheel (Fig. 1b). In cell-based orientation maps (see Methods), we plotted the preferred orientation of each neuron and found that orientation varied smoothly over the cortical surface with very little scatter (Fig. 1c–e). In the experiment illustrated in Fig. 1b, c, data were collected at nine depths spanning 160 μm . When cells from all depths were superimposed (Fig. 1c, lower right; see also Supplementary Video 1), the orientation maps matched precisely and the pinwheel centre was immediately evident. This demonstrates the columnar structure of the orientation map at a very fine spatial scale. Even near the pinwheel centre there was virtually no mixing of cells with different orientation preferences.

The orientation tuning of individual neurons is best appreciated by examining the time course of the calcium signals evoked by visual stimulation (see also Supplementary Video 2 for a time-lapse movie of the calcium signal changes). Figure 2 shows three examples of individual neurons close to a pinwheel centre (less than 65 μm , Fig. 2b) and in an iso-orientation domain at some distance from the centre (more than 65 μm , Fig. 2c). The radius of 65 μm (Fig. 2a) was chosen to approximate the recording sphere of the multi-electrodes (tetrodes) used in earlier studies¹⁴. As shown previously (Fig. 2 in ref. 6), the preferred orientations of the cells close to the pinwheel centre were frequently very different from each other (Fig. 2d); for instance, cells 1 and 3 (Fig. 2b) were tuned to orthogonal orientations. In contrast, cells in a neighbourhood of the same diameter in the iso-orientation domain (Fig. 2e) were all tuned to nearly identical orientations.

We examined 6,616 cells from ten pinwheels in nine animals (2–17 depths were imaged for each pinwheel). In all, 1,002 cells were located in what we call the pinwheel centre (less than 65 μm from the singularity; see Supplementary Methods). Of these, 796 (79.4%) were selective for orientation, 41 (4.1%) were non-selective but responsive, and 165 (16.5%) were unresponsive. In the periphery (more than 65 μm from the centre), out of 5,614 cells, 5,230 (93.2%) were selective, 59 (1.1%) were non-selective but responsive, and 325 (5.8%) were unresponsive.

To demonstrate that the preferred orientations of cells changed smoothly and progressively around the pinwheel, the preferred orientations of all selective cells for each pinwheel were plotted against the azimuth (θ in Fig. 3a), the angular positions of cells with respect to the pinwheel centre (Fig. 3b). As illustrated in Fig. 1c, the relation between the cells’ preferred orientation and angular positions was well fitted by a smooth curve (black curve in Fig. 3b, the

¹Department of Neurobiology, Harvard Medical School, Boston, Massachusetts 02115, USA. ²Max Planck Institute of Neurobiology, D-82152 Munich-Martinsried, Germany.

†Present addresses: Center for Neural Science, Korea Institute of Science and Technology, Seoul 136-791, South Korea (S.C.); Department of Neuroscience, Medical University of South Carolina, Charleston, South Carolina 29425, USA (P.K.).

azimuth–orientation function) derived from cells located in the periphery of the pinwheel (more than $65\ \mu\text{m}$ from the centre; blue points). Cells in the pinwheel centre (less than $65\ \mu\text{m}$; red points) follow the same curve (correlation coefficient $r = 0.98$). Thus, cells in the centre of the pinwheel are arranged according to the pattern seen in the periphery.

We further examined the relationship between pinwheel centre and periphery by quantifying three parameters: the orderliness of the orientation map, the response strength, and the orientation tuning width. First, we measured the angular deviation, which is the degree to which individual cells deviated from the orderly pinwheel arrangement, expressed in the azimuth–orientation function (black curve in Fig. 3b) for each pinwheel. For cells close to the pinwheel centre, the distribution of angular deviations was clearly biased towards zero (Fig. 3c; median 9°), although they were somewhat higher than in the surround (Fig. 3d; median 5° (see also Supplementary Fig. S2); however, if the deviation was measured as cortical displacement of neurons, it was smaller at the centre (see Supplementary Fig. S3)). The distribution in the centre was significantly different from the random distribution obtained by shuffling the location of cells (Fig. 3c, grey bars; $P < 10^{-10}$; Wilcoxon rank-sum test). Second, the response amplitudes in the pinwheel centre (Fig. 3f; median 4.3% fluorescence increase) were smaller than in the periphery (Fig. 3g; 5.8%, $P < 10^{-12}$; Wilcoxon rank-sum test). Finally, cells close to the pinwheel centre were selective to orientation but had a slightly broader tuning bandwidth (Fig. 3i; median 37°) than cells in the periphery (Fig. 3j; median 31° ; $P < 10^{-4}$; Wilcoxon rank-sum test). The differences in tuning width were sufficiently robust that they were observed independently in different subsets of the data (even and odd trials, Supplementary Figs S4 and S5).

We found essentially the same relationship between the pinwheel centre and periphery in all ten pinwheels studied. The pinwheel

centres were remarkably well organized: the median angular deviation of the measured preferred orientation from the azimuth–orientation function was small (less than 17°), although consistently larger than in the periphery (Fig. 3e). The median response strength of the cells was always 17–41% smaller in the pinwheel centre than in the periphery (Fig. 3h). The median bandwidth of orientation tuning was consistently broader in the pinwheel centre than in the periphery, but this difference was always small (less than 11° ; Fig. 3k).

The present study was performed with kittens at an age when orientation maps are well established (postnatal days 28–35)^{15,16}, but still within the critical period. Our results are consistent with the idea that tuning width might be slightly broader in the pinwheel centres of kittens of this age, as has been suggested¹⁷. However, any quantitative conclusions about the degree of orientation tuning must take several technical issues into consideration. First, to minimize experiment time, we sampled orientation coarsely (45°) in most experiments. When we sampled orientation more densely (22.5°) in some experiments, the apparent tuning width of the most selective cells became considerably smaller (see Supplementary Figs S6 and S7), which rather enlarged the difference in tuning width between centre and periphery. Second, the smaller responses at the pinwheel centres might result in apparently broader curves due to decreased signal-to-noise ratios; indeed, the measured tuning width was inversely correlated with response strength both near the centre and in the periphery (Supplementary Fig. S8).

The smaller responses near the pinwheel centres than in the periphery might also have contributed to the apparently higher percentage of unresponsive cells in the centre (16.5%) than in the periphery (5.8%). Alternatively, the unresponsive cells at the pinwheel centres might have been selective to some other stimulus attributes. In a few experiments we tried square-wave gratings at a range of spatial frequencies (0.07–1.0 cycles/degree) at a single

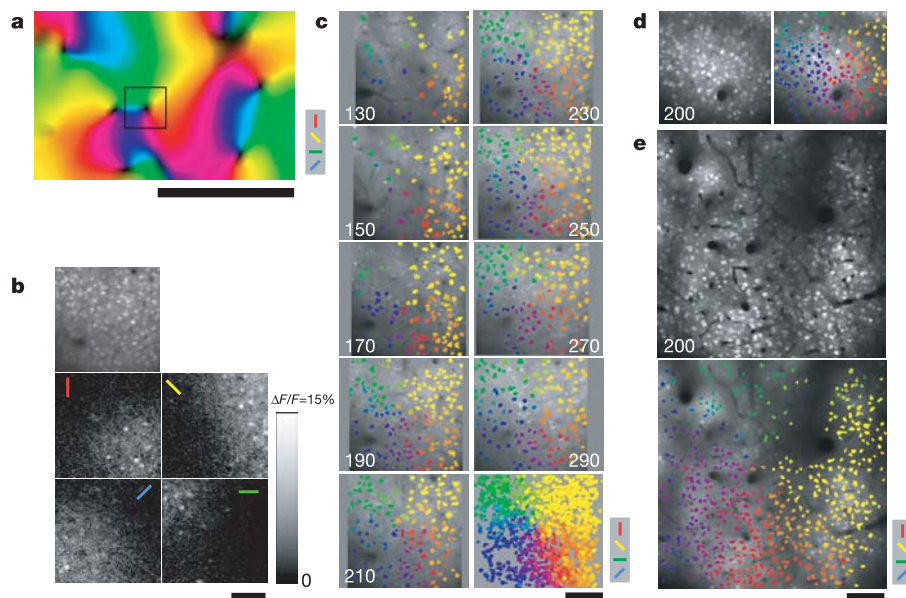


Figure 1 | Functional maps of orientation pinwheels. Pinwheels were mapped at low resolution (**a**) and with single-cell resolution (**b–e**). **a**, An orientation map obtained with intrinsic-signal optical imaging. In this colour-coded map (polar map), hue is determined by the best orientation. Darker colours, in pinwheel centres, represent less selective responses. **b**, Two-photon calcium imaging. Approximately, the square region drawn in **a** was imaged at $250\ \mu\text{m}$ below the pial surface. The top panel shows an averaged image of cortical cells stained with the calcium indicator Oregon Green 488 BAPTA-1 AM. The bottom four panels show single-condition maps for four orientations of visual stimuli ($\Delta F/F$, the percentage change in fluorescence between stimulation period and blank; gaussian smoothed

by $1\ \mu\text{m}$). The scale bar ($\Delta F/F$) applies only to the bottom four panels. **c**, Cell-based orientation maps from nine different depths (130, 150, 170, 190, 210, 230, 250, 270 and $290\ \mu\text{m}$, as indicated). Selective cells (1,034 out of 1,055 cells; $P < 0.05$, ANOVA across eight directions) are coloured according to their preferred orientation. The cortical surface was tilted (about 15°), which was corrected for by shifting the images by $5.2\ \mu\text{m}$ for every $20\ \mu\text{m}$ in depth (grey margins indicate this shift). The last panel shows the overlay of images from all nine depths. **d**, **e**, Dye-loaded cells and orientation maps in pinwheels from two other animals. Scale bars, 1 mm (**a**); $100\ \mu\text{m}$ (**b–e**).

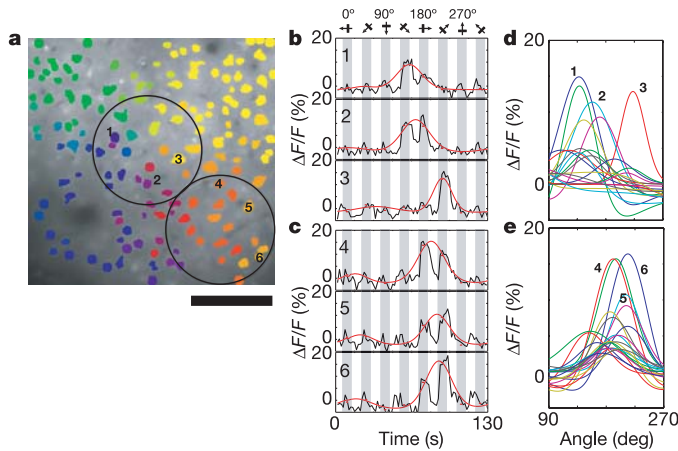


Figure 2 | Tuning curves of cells close to a pinwheel centre and in an iso-orientation domain. **a**, A cell-based orientation map from 230 μm below the pial surface (redrawn from Fig. 1c). Cells were sampled from two circular regions (radius 65 μm), one at the pinwheel centre and the other in an iso-orientation domain. Scale bar, 100 μm . **b**, **c**, Time courses of three selective cells (1–3) in the pinwheel centre (**b**) and three selective cells (4–6) in the iso-orientation domain (**c**). Grey bars indicate periods of visual stimulation—oriented gratings drifted in eight directions—which were interspersed with blank stimuli of uniform luminance. Black traces show the average response to ten repeats; red traces show the orientation tuning curves fitted to the peak responses. **d**, **e**, Tuning curves of all the cells in the pinwheel centre (**d**) and the iso-orientation domain (**e**). Tuning curves of cells 1–6 are numbered.

orientation, but observed similar results. We did not examine whether more complex stimuli, such as corners or other contextual influences¹⁸, might preferentially excite neurons in pinwheel centres.

Previously we reported the existence of precise borders¹⁰—direction fractures—between cells with opposite direction preferences in cat area 18. In theory, direction fractures must intersect with pinwheel

centres because one cycle of orientation (180°) cannot span a full cycle of directions (360°; see refs 19–21). In seven out of ten pinwheels we examined, a well-defined direction fracture intersected the pinwheel centre (Supplementary Fig. S9). In the other three cases, the arrangement was less clear.

Two-photon calcium imaging is unique in its ability to determine not only the physiological response of hundreds of cells simultaneously but also their precise location in the cortical circuit. This enabled us to explore the functional micro-architecture of orientation pinwheels in cat visual cortex and to prove that pinwheel centres truly represent singularities in the cortical orientation map. These singularities are substantially different from a linear border, such as a direction fracture^{10,20,21}. With a linear border, if a neuron’s dendritic arbour is symmetric, more than half will overlap cells with similar properties. Near a pinwheel centre, however, any symmetric dendritic arbour would overlap predominantly with regions of different orientation preferences.

Several different mechanisms might be responsible for the sharp orientation tuning of neurons near the pinwheel centre, despite the fact that most of their nearest neighbours have different orientation preferences. First, the cell bodies in the centre of pinwheels might have dendrites that are strongly biased towards the nearby domain with the same orientation (Supplementary Fig. S10a). Alternatively, the overall dendritic arbour might be symmetric, with little or no bias, but there could be stronger or more numerous synapses along dendrites in the iso-orientation domain (Supplementary Fig. S10b). Even with symmetric inputs around the dendritic tree, however, sharp tuning could still be achieved. If synapses proximal to cell bodies were stronger than distal synapses (Supplementary Fig. S10c), then neurons only slightly displaced from the centre would be sharply tuned, provided that local afferent inputs are themselves tightly segregated. Finally, even if symmetric neurons integrated inputs over a large dendritic area (Supplementary Fig. S10d), weakly biased orientation tuning could be sharpened by a nonlinear input–output transformation, such as the threshold for spike generation^{7,22}.

With any one of these mechanisms of sharp orientation tuning, the

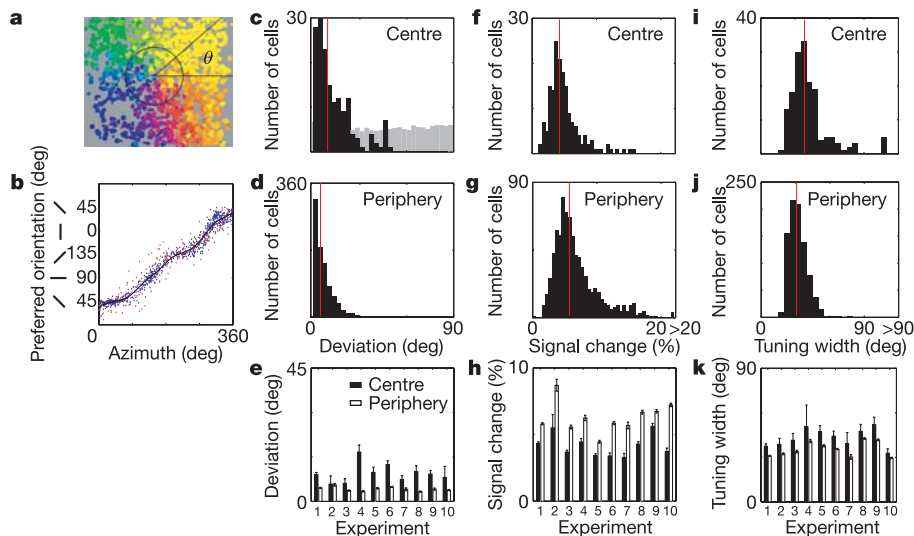


Figure 3 | Relationship between neurons in the pinwheel centre (less than 65 μm from singularity) and in the periphery (more than 65 μm). **a**, An overlay of cell-based orientation maps from nine depths (redrawn from Fig. 1c). **b**, Relation between cell positions (azimuth; defined as θ in **a**) and the preferred orientations. Red dots represent cells in the pinwheel centre, blue dots in the periphery. All selective cells (1,034 out of 1,055 cells from nine depths) are included. The azimuth–orientation function (black trace) was obtained by fitting the blue dots with a smooth curve. **c**, **d**, Histograms of angular deviation of preferred orientation from the average (black trace) in **b** for all the selective cells near the pinwheel centre

(**c**) and in the periphery (**d**). The grey histogram in **c** shows the random distribution obtained by shuffling the location of cells. Red lines, median values (see the text). **e**, Median angular deviation for cells in the pinwheel centre (filled bars) and the periphery (open bars) for all ten pinwheels studied. **f**, **g**, Histograms of change in fluorescence evoked by optimal orientation near the pinwheel centre (**f**) and in the periphery (**g**). **h**, Median signal changes in all pinwheels. **i**, **j**, Histograms of tuning width (half-width at half-maximum) for all the cells near the pinwheel centre (**i**) and in the periphery (**j**). **k**, Median tuning widths in all pinwheels. Where shown, error bars indicate s.e.m.

question would still remain: what is the developmental process that yields the precise arrangement of neurons in a pinwheel centre? It is known that the macroscopic architecture of pinwheels is established by the time of eye opening in the ferret²³ and is stable throughout the critical period in the cat^{15,16}. If neurons received many inputs over large dendritic arbours, then their outputs would represent a smooth interpolation of the macroscopic map. Thus, a pinwheel centre could be spatially precise even if each cell is broadly tuned early in development¹⁷. The sharpening of their orientation tuning could then be achieved by hebbian mechanisms that might, for instance, selectively prune dendritic arbours (Supplementary Fig. S10a) or strengthen specific synaptic connections (Supplementary Fig. S10b). Alternatively, the broadly tuned inputs in the pinwheel centre might be sharpened in the adult by a threshold operation, so there is no need for morphological or synaptic refinement to achieve sharp tuning⁷ (Supplementary Fig. S10d).

The discovery of macroscopic functional architecture initiated studies of the relationship between function and morphology of axonal arbours (see, for example, refs 24, 25) and dendritic trees^{26–29}. The demonstration of precise micro-architecture in the present study suggests a relationship between functional maps and anatomy at an even finer spatial scale. Neuronal operations at this scale will be understood only when microscopic functional imaging is combined with higher-resolution techniques that elucidate neuronal morphology and perhaps even individual synaptic connections.

METHODS

Cats (postnatal days 28–35) were anaesthetized with isoflurane (1–2% in surgery, 0.5–1% during imaging; see Supplementary Methods for details). A small craniotomy was performed over the visual cortex, the dura reflected and the underlying cortex covered with 3% agarose. For intrinsic-signal optical imaging, the cortex was illuminated with 630-nm light and the camera (Imager 3001; Optical Imaging) was focused 400 μm below the cortical surface. Using the surface blood vessel pattern, we targeted a pinwheel centre with a glass pipette to inject the cell-permeant calcium indicator (0.8 mM Oregon Green 488 BAPTA-1 AM with 8% dimethylsulphoxide, 2% pluronic acid and 40 μM Alexa-594; all from Molecular Probes). Changes in calcium fluorescence of cortical neurons were monitored with a Leica TCS SP2 microscope coupled with a Mira 900 (Coherent Systems) mode-locked Ti:sapphire laser (810 nm). For visual stimulation, square-wave gratings were drifted at 2 Hz at 8 or 16 directions of motion in steps of 22.5° or 45°. Each stimulus started with a blank period (8 s) followed by the same period of visual stimulation. The 8 or 16 stimuli were presented sequentially and repeated 10 times. Two-photon images were analysed in Matlab (Mathworks) and ImageJ (National Institutes of Health). Cells were automatically identified (6,616 cells in 10 pinwheels) through a series of morphological filters that delineated the contours of cell bodies. Visually responsive cells were defined by analysis of variance (ANOVA) across the blank and 8 or 16 directions ($P < 0.05$; 6,126 cells, 92.6%). Of these, selective cells were defined by ANOVA across 8 or 16 directions ($P < 0.05$; 6,026 cells, 91.1%). Preferred orientation was obtained by vector averaging. Tuning curves were fitted with the sum of two circular gaussian functions³⁰.

Received 5 April; accepted 28 June 2006.

Published online 13 August 2006.

- Hubel, D. H. & Wiesel, T. N. Shape and arrangement of columns in cat's striate cortex. *J. Physiol. (Lond.)* **165**, 559–568 (1963).
- Hubel, D. H. & Wiesel, T. N. Sequence regularity and geometry of orientation columns in the monkey striate cortex. *J. Comp. Neurol.* **158**, 267–293 (1974).
- Blasdel, G. G. & Salama, G. Voltage-sensitive dyes reveal a modular organization in monkey striate cortex. *Nature* **321**, 579–585 (1986).
- Grinvald, A., Lieke, E., Frostig, R. D., Gilbert, C. D. & Wiesel, T. N. Functional architecture of cortex revealed by optical imaging of intrinsic signals. *Nature* **324**, 361–364 (1986).
- Bonhoeffer, T. & Grinvald, A. Iso-orientation domains in cat visual cortex are arranged in pinwheel-like patterns. *Nature* **353**, 429–431 (1991).
- Maldonado, P. E., Gödecke, I., Gray, C. M. & Bonhoeffer, T. Orientation selectivity in pinwheel centres in cat striate cortex. *Science* **276**, 1551–1555 (1997).

- Schummers, J., Marino, J. & Sur, M. Synaptic integration by V1 neurons depends on location within the orientation map. *Neuron* **36**, 969–978 (2002).
- Svoboda, K., Denk, W., Kleinfeld, D. & Tank, D. W. *In vivo* dendritic calcium dynamics in neocortical pyramidal neurons. *Nature* **385**, 161–165 (1997).
- Stosiek, C., Garaschuk, O., Holthoff, K. & Konnerth, A. *In vivo* two-photon calcium imaging of neuronal networks. *Proc. Natl Acad. Sci. USA* **100**, 7319–7324 (2003).
- Ohki, K., Chung, S., Ch'ng, Y. H., Kara, P. & Reid, R. C. Functional imaging with cellular resolution reveals precise micro-architecture in visual cortex. *Nature* **433**, 597–603 (2005).
- Sullivan, M. R., Nimmerjahn, A., Sarkisov, D. V., Helmchen, F. & Wang, S. S. *In vivo* calcium imaging of circuit activity in cerebellar cortex. *J. Neurophysiol.* **94**, 1636–1644 (2005).
- Kerr, J. N., Greenberg, D. & Helmchen, F. Imaging input and output of neocortical networks *in vivo*. *Proc. Natl Acad. Sci. USA* **102**, 14063–14068 (2005).
- Meister, M. & Bonhoeffer, T. Tuning and topography in an odor map on the rat olfactory bulb. *J. Neurosci.* **21**, 1351–1360 (2001).
- Gray, C. M., Maldonado, P. E., Wilson, M. & McNaughton, B. Tetrapodes markedly improve the reliability and yield of multiple single-unit isolation from multi-unit recordings in cat striate cortex. *J. Neurosci. Methods* **63**, 43–54 (1995).
- Gödecke, I., Kim, D. S., Bonhoeffer, T. & Singer, W. Development of orientation preference maps in area 18 of kitten visual cortex. *Eur. J. Neurosci.* **9**, 1754–1762 (1997).
- Crair, M. C., Gillespie, D. C. & Stryker, M. P. The role of visual experience in the development of columns in cat visual cortex. *Science* **279**, 566–570 (1998).
- Crair, M. C., Ruthazer, E. S., Gillespie, D. C. & Stryker, M. P. Relationship between the ocular dominance and orientation maps in visual cortex of monocularly deprived cats. *Neuron* **19**, 307–318 (1997).
- Das, A. & Gilbert, C. D. Topography of contextual modulations mediated by short-range interactions in primary visual cortex. *Nature* **399**, 655–661 (1999).
- Swindale, N. V., Matsubara, J. A. & Cynader, M. S. Surface organization of orientation and direction selectivity in cat area 18. *J. Neurosci.* **7**, 1414–1427 (1987).
- Weliky, M., Bosking, W. H. & Fitzpatrick, D. A systematic map of direction preference in primary visual cortex. *Nature* **379**, 725–728 (1996).
- Shmuel, A. & Grinvald, A. Functional organization for direction of motion and its relationship to orientation maps in cat area 18. *J. Neurosci.* **16**, 6945–6964 (1996).
- Marino, J. *et al.* Invariant computations in local cortical networks with balanced excitation and inhibition. *Nature Neurosci.* **8**, 194–201 (2005).
- Chapman, B., Stryker, M. P. & Bonhoeffer, T. Development of orientation preference maps in ferret primary visual cortex. *J. Neurosci.* **16**, 6443–6453 (1996).
- Gilbert, C. D. & Wiesel, T. N. Columnar specificity of intrinsic horizontal and corticocortical connections in cat visual cortex. *J. Neurosci.* **9**, 2432–2442 (1989).
- Mooser, F., Bosking, W. H. & Fitzpatrick, D. A morphological basis for orientation tuning in primary visual cortex. *Nature Neurosci.* **7**, 872–879 (2004).
- Katz, L. C., Gilbert, C. D. & Wiesel, T. N. Local circuits and ocular dominance columns in monkey striate cortex. *J. Neurosci.* **9**, 1389–1399 (1989).
- Hübener, M. & Bolz, J. Relationships between dendritic morphology and cytochrome oxidase compartments in monkey striate cortex. *J. Comp. Neurol.* **324**, 67–80 (1992).
- Kossel, A., Löwel, S. & Bolz, J. Relationships between dendritic fields and functional architecture in striate cortex of normal and visually deprived cats. *J. Neurosci.* **15**, 3913–3926 (1995).
- Hickmott, P. W. & Merzenich, M. M. Dendritic bias of neurons in rat somatosensory cortex associated with a functional boundary. *J. Comp. Neurol.* **409**, 385–399 (1999).
- Swindale, N. V., Grinvald, A. & Shmuel, A. The spatial pattern of response magnitude and selectivity for orientation and direction in cat visual cortex. *Cereb. Cortex* **13**, 225–238 (2003).

Supplementary Information is linked to the online version of the paper at www.nature.com/nature.

Acknowledgements We thank S. Yurgenson for technical support and programming, A. Kerlin for programming, and A. Vagodny for surgical assistance. This work was supported by grants from the NIH, the Lefler Fund, the Goldenson/Berenberg Fund, and the Max Planck Society.

Author Information Reprints and permissions information is available at www.nature.com/reprints. The authors declare no competing financial interests. Correspondence and requests for materials should be addressed to R.C.R. (clay_reid@hms.harvard.edu).